

## Study on Underwater Friction Stir Welding of AA7075-T651

Robert Kosturek<sup>1\*</sup>, Janusz Torzewski<sup>1</sup>, Lucjan Śniezek<sup>1</sup>

<sup>1</sup> Department of Fatigue and Machine Design, Faculty of Mechanical Engineering, Military University of Technology, gen. S. Kaliskiego 2 Str., Warsaw, Poland

\* Corresponding author's e-mail: robert.kosturek@wat.edu.pl

### ABSTRACT

This study examines the application of additional water cooling on the mechanical properties of AA7075-T651 alloy friction stir welded butt joints. Underwater joints were produced in a wide range of welding parameters and compared to conventional FSW joints in terms of microhardness and basic mechanical properties. The low-cycle fatigue properties of selected FSW and UWFSW joints were also compared. It was stated that regardless of the welding parameters used, UWFSW joints outperform conventional FSW joints of the AA7075-T651 alloy in terms of YS and UTS, with only a slightly lower ductility. The use of machining coolant enables the production of UWFSW joints with a higher load-carrying capacity, including a 15% increase in YS, a 10% increase in UTS, and approximately a 5% increase in ductility compared to FSW. Under low-cycle fatigue conditions, UWFSW joints exhibit a greater tendency for cyclic hardening, lower plastic strain amplitude, and fewer cycles to failure.

**Keywords:** friction stir welding, aluminium, mechanical properties, fatigue, underwater welding, cooling.

### INTRODUCTION

The development of friction stir welding (FSW) technology and its application to joining high-strength aluminium alloys significantly influenced light construction manufacturing. In recent years, FSW has been used in i.a. production of fuel tanks [1], and space shuttles (e.g. NASA's Orion Spacecraft) [2]. The basic idea of the process is to locally plasticize workpieces material and stir them together to form a joint. It is achieved by putting between the edges of plates to be welded a specially designed, rotating tool, which by friction heats and mechanically mixes the softened material [3]. For the temperature of plasticization is a function of melting point [4], the FSW technique is predominantly applied in industry to weld aluminium and magnesium alloys [5], and to some extent, copper alloys [6]. Besides the most basic, technological, advantages in welding aluminium, such as lack of porosity, no requirement of filler and gas shielding, and no risk of hot cracking, the hot deformation in the stirred region creates ultrafine,

dynamically-recrystallized, microstructure, providing excellent mechanical properties [7]. The most crucial area, determining the entire joint load-carrying capacity, is the so-called low-hardness zone (LHZ), which depending on welding parameters can be located in the heat-affected zone (HAZ)/thermo-mechanically affected zone (TMAZ) boundary, in TMAZ or the stir zone (SZ) [8]. When it comes to precipitation-hardened aluminium alloys, the heat-initiated adverse evolutions of the strengthening phase, reduce ultimate tensile strength (UTS) by about 15-25%, depending on the alloy [9].

To limit this deterioration in joint's performance, some modifications of FSW [10, 11] and post-processing have been proposed [12]. One of the most promising solutions, in terms of its simplicity and efficiency, is underwater friction stir welding (UWFSW). The use of an additional cooling medium allows for the rapid dissipation of excess heat from the welded plate, and consequently, it limits the impact of the welding process on the distribution of the strengthening phase in the joined alloy [13]. Moreover, in comparison

with FSW, UWFSW results in additional refinement of grain size in the SZ due to low peak temperature and its low duration [13]. Additionally, it is worth mentioning the technological aspect of UWFSW, which involves manufacturing joints of 5XXX alloys used in shipbuilding, particularly in a wet dock environment [14]. The UWFSW process can also be applied to low-carbon steel joining with a potential 20% increase in the UTS compared to the conventional FSW [15].

Recent studies on UWFSW of high-strength aluminium alloys have primarily focused on the 2XXX alloy series. Sree Sabari et al. investigated the influence of tool rotation speed on mechanical properties of 6 mm thick armour grade AA2519-T87 alloy FSW and UWFSW joints [16]. Comparing the highest achieved FSW and UWFSW joint efficiencies, the authors stated that the underwater variant allowed to improve joint efficiency by 20% (about 90 MPa in the UTS) [16]. Liu et al. focused on the UWFSW of 7.5 mm thick AA2219-T62 alloy, achieving the UTS of 347 MPa, corresponding to 80% of that of the base material [17]. The authors also reported that the improvement in mechanical properties is observed by increasing welding velocity within the range of 50 to 150 mm/min, and further increase to 200 mm/min resulted in their decrease [17]. The same alloy and its thickness was researched by Zhang et al. in terms of the relationship between tool rotation speed and mechanical properties of UWFSW joints at the fixed welding speed of 100 mm/min [18]. It was reported that with increasing rotation speed, the tensile strength first increased from 600 to 800 rpm, then reached a plateau between 800 and 1200 rpm, to sharply decreased at 1400 rpm due to the void defect formation [18]. Although it gives a general look on the optimal set of process parameters (in terms of joint's efficiency), it has to be noted that it also strongly depends on the type of used tool and plate thickness. Rouzbehani et al. joined 5 mm thick Al7075 alloy using the UWFSW process in a broad range of welding parameters [19]. The

authors discovered that in every set of parameters, the UTS of the UWFSW joint is about 7–10% higher than for air-cooled FSW [19]. Additionally, it was reported that UWFSW joints are more susceptible to form a defect in the bottom part of the weld for higher tool traverse speed values [19]. When considering the application of UWFSW joints in structures subjected to cyclic loads, it is crucial to examine their fatigue properties [20]. A study examining the fatigue properties of the 6 mm thick AA2219-T62 UWFSW joint was conducted by Xu et al. [21]. It was stated that the UWFSW joints have higher stress amplitude and fatigue life than their air-cooled counterparts [21]. An additional factor that may improve the strength of UWFSW joints under variable load conditions is the presence of lower residual stresses compared to conventional FSW joints [22].

In this investigation, the material to be examined is AA7075-T651 alloy, a high-strength aluminium alloy, widely used in i.a. aerospace and military industry [23]. For a high concentration of alloying elements significantly limits its weldability by conventional means, the implantation of the FSW technique was a huge step forward in joining of AA7075 alloy. Although the FSW resolved many difficulties in this field, the high sensitivity of the strengthening phases to temperature results in relatively low joint efficiencies [25]. In a previous study performed by authors on 5 mm thick AA7075-T651, it was reported that it is possible to achieve FSW joint efficiency of 76% (447 MPa) [25]. This investigation is a continuation of that study and aims to examine in a broad range of welding parameters the influence of the UWFSW process on the mechanical properties of AA7075-T651 alloy.

## MATERIALS AND METHODS

The chemical composition (tab. 1) and basic mechanical properties (Tab. 2) of AA7075-T651 alloy used in this investigation are presented in the tables

**Table 1.** Chemical composition of AA7075-T651 alloy (% weight)

Si	Fe	Cu	Mn	Mg	Cr	Zn	Ti	Al
0.071	0.122	1.610	0.025	2.596	0.197	5.689	0.041	Base

**Table 2.** Mechanical properties of AA7075-T651 alloy

Yield strength, $R_{0.2}$	Tensile strength, $R_m$	Elongation at break, A	Microhardness
547.5 ± 1.3 MPa	583.5 ± 1 MPa	14.4 ± 0.6 %	170 ± 3.59 HV0.1

below. The presented composition has been provided by alloy's supplier (BIKAR-Metalle GmbH).

The 5 mm thick AA7075-T651 plate was cut into 80×500 mm pieces. Before the welding, the upper surfaces of the plates were machined and washed with isopropyl alcohol to remove the oxide layer and degrease them. The welding process was performed on ESAB FSW Legio 4UT (Fig. 1). A specially designed work table provides the possibility of welding in underwater conditions. The constant welding parameters were: 2° tool tilt angle and 4.8 mm tool penetration depth. The tool used for manufacturing joints to be investigated was 0810134-001 (ESAB catalogue number). The welding was conducted in a direction perpendicular to the rolling direction. In total eleven joints were made with various sets of

tool rotation speed, welding velocity, and cooling media (Table 3).

The proposed matrix was the result of a previous investigation performed by authors [25]. The initial water temperature was about 20°C and its layer height over the workpiece upper surface was 15 mm. One of the joints produced via 400 rpm / 100 mm/min set of welding parameters was manufactured additionally with machining coolant, the water solution of 10% Blaser Blasocut 2000. The air-cooled joint is a conventional friction stir welded joint, and it was placed in this study for comparison purposes. The data presented for this joint are taken from the previous study [25]. All joints presented in this study were visually inspected, and no defects were found. For macrostructure observations, samples were cut



Figure 1. ESAB FSW Legio 4UT

Table 3. Welding parameters and samples designation

Sample	Welding parameters		
	Tool rotation speed	Tool traverse speed	Cooling medium
405	400 rpm	50 mm/min	Water
410-A		100 mm/min	Air
410			Water
410-B			Machining coolant
415		150 mm/min	Water
605	600 rpm	50 mm/min	
610		100 mm/min	
615		150 mm/min	
805	800 rpm	50 mm/min	
810		100 mm/min	
815		150 mm/min	

from the welded plates and subjected to standard metallographic preparation, which included mounting in resin, grinding, polishing, and etching. The used etchant was Keller’s reagent with the following composition: 20 ml H<sub>2</sub>O, 5 ml of 63% HNO<sub>3</sub>, 1 ml of 40% HF, 2 drops of 36% HCl, and about 10 s etching time. The observations were conducted on the OLYMPUS LEXT OLS4100 microscope. The manufactured joints were also subjected to microhardness measurements using a Struers DURA SCAN 70 with an applied load of 0.98 N and a loading time of 10 s. The microhardness distributions were obtained on each joint’s cross-section in its middle height (2.5 mm from a welded plate upper surface). In order to evaluate the mechanical performance of produced welded joints, the tensile tests were carried out on INSTRON 8802 MTL universal testing machine in accordance with the ASTM standard E8/E8M–13a [26]. The machine is equipped with specialized LCF testing software provided by Instron. For each sample, three tensile tests were conducted. All error bars presented in this study represent the standard deviation. The

schemes of specimens used in this experiment are presented in Fig. 2.

For comparison of fatigue properties the samples 410-A and 410-B were subjected to the strain-controlled low cycle fatigue testing in accordance with the ISO standard 12106:2017 [27]. The cycle asymmetry ratio was equal to R=0.1 and the tested total strain amplitudes were  $\epsilon_{ac} = 0.35, 0.4, 0.5, \text{ and } 0.6\%$ . Strain measurement during LCF was carried out using the Instron 2620-603 Dynamic Extensometer with a 25 mm gauge length  $\pm 4\%$  axial travel.

## RESULTS AND DISCUSSION

### Macrostructural observations

As part of the investigation, the macrostructural observations have been conducted. The images of the selected, extreme samples are presented in Fig. 3a-d. In all cases, obtained joint are defect-free, and despite the presence of additional

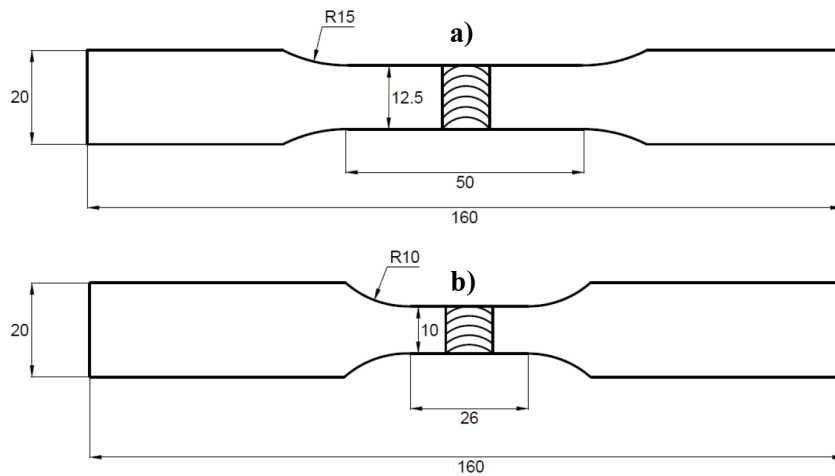


Figure 2. Scheme of the specimens for tensile (a) and low-cycle fatigue (b) testing

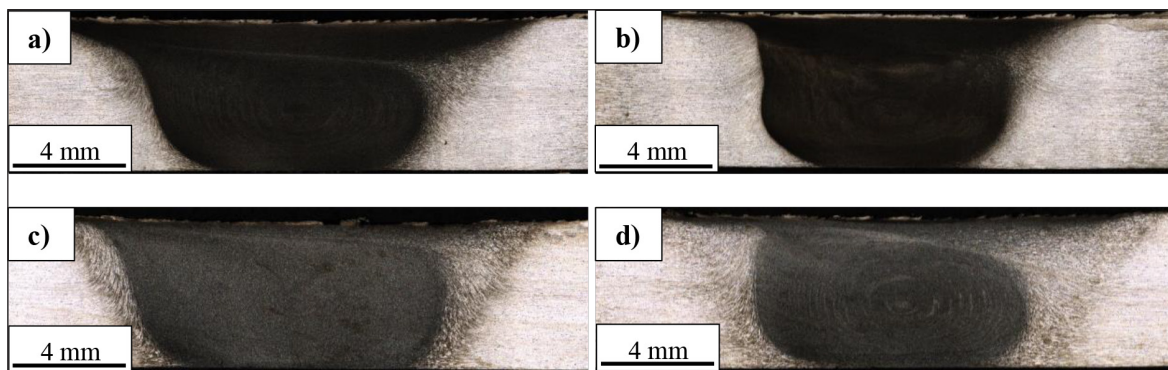


Figure 3. Macrostructural images of samples: 405 (a), 415 (b), 805 (c), 815 (d)

cooling medium, the material in the bottom part of the workpiece was plasticized and mixed. Most likely the kissing bond defect would occur in the sample with the lowest heat input (Fig. 4b), but no presence of such imperfection is stated. Another type of potential defect that could be formed as the result of water cooling is voids. They are created, among others, in the condition of significant differences in temperature between the bottom and the upper part of the stirred material [28]. It often occurs where there is a high ratio of tool rotation speed to tool traverse speed, like in the case of the 815 sample (Fig. 3d), which, similar to all other samples, is defect-free. Some tendencies, typical for the FSW joints, are possible to observe, like the narrowing of the SZ while increasing tool traverse speed (Fig. 3a and 3b, 3c and 3d). Measuring the width of the SZ at the joint's mid-thickness it can be stated that the reduction for the samples produced with 400 rpm tool rotation speed is about 11% (Fig. 3a,b), while for their 800 rpm counterpart it equals 8% (Fig. 3c,d). The samples welded with 800 rpm tool rotation speed are generally characterized by an 8% wider SZ than 400 rpm samples.

### Microhardness analysis

The obtained microhardness distribution on joint's cross-sections are presented in Fig. 4a-d. The obtained microhardness distributions are characteristic in shape for FSW joints of a precipitation-hardened aluminium alloy. Plastic deformation at elevated temperatures leads to a decrease in the degree of strengthening of the AA7075-T651 alloy due to the overaging of the strengthening phase. In the SZ, a dynamically recrystallized, fine-grained microstructure is formed, which results in additional strengthening by grain boundaries, somewhat compensating for the loss in the content of the strengthening phase. Analysing the distributions obtained for joints produced at a rotational speed of 400 rpm with water cooling, one can observe the effect of tool traverse speed on the welded material (Fig. 4a). The most significant aspect of increasing the tool traverse speed is the reduction of heat affecting the joined material, which directly results in a narrower HAZ. The recorded hardness of the LHZ is approximately 130 HV0.1, and depending on the welding speed, it is located closer to or further from the centre of the joint. At the same time, certain features of the hardness distributions of these joints differ from

their underwater counterparts at 600 rpm (Fig. 4b) and 800 rpm (Fig. 4c). In the case of the 400 rpm joints, it can be observed that increasing the welding speed results in a decrease in the hardness of the SZ (Fig. 4a), which is the opposite of the trends observed for the other samples (Fig. 4b, c). The underwater joints at 600 and 800 rpm are also characterized by higher weld zone hardness, ranging between 146-164 HV0.1, depending on the welding speed used. The higher peak temperature is generally accompanied by higher SZ hardness, due to more efficient dissolution of alloying elements into the matrix, which can re-precipitate during the cooling stage [29]. Both 600 and 800 rpm samples also exhibit similar hardness values in the HAZ, which vary depending on the welding speed: 120 HV0.1 (50 mm/min), 125 HV0.1 (100 mm/min), and 132 HV0.1 (150 mm/min). Interestingly, when compared to sample 415, samples 615 and 815 showed higher LHZ hardness, despite their corresponding welding parameters involved a higher heat input. A similar trend has been observed for air-cooled FSW joints of AA2519-T62 alloy, welded with 100 mm/min tool traverse speed [8]. All samples produced using 100 mm/min welding speed are set in Fig. 4d. First and foremost, one can observe the significant impact of water cooling on the microhardness distribution when comparing samples 410-A and 410. The sample produced with air cooling features a noticeably wider HAZ (reaching up to 15 mm from the centre of the joint), a lower LHZ hardness (approximately 115 HV0.1), at the same time, exhibiting a higher SZ hardness (averaging around 145 HV0.1). Sample 410-B, cooled using machining coolant, is situated somewhat between the hardness profiles of samples 410-A and 410. Despite having a microhardness in the LHZ similar to that of sample 410 (approximately 125 HV0.1), sample 410-B exhibits a noticeably higher SZ hardness (around 145 HV0.1) and a wider HAZ. This suggests that, in the UWFSW process, the use of machining coolant results in less effective heat dissipation compared to using pure water. Analysis of the remaining distributions confirms the previously observed relationship between the SZ hardness and tool rotational speed (Fig. 4d).

### Tensile test

In order to evaluate the load-carrying capabilities of the produced samples and the influence of

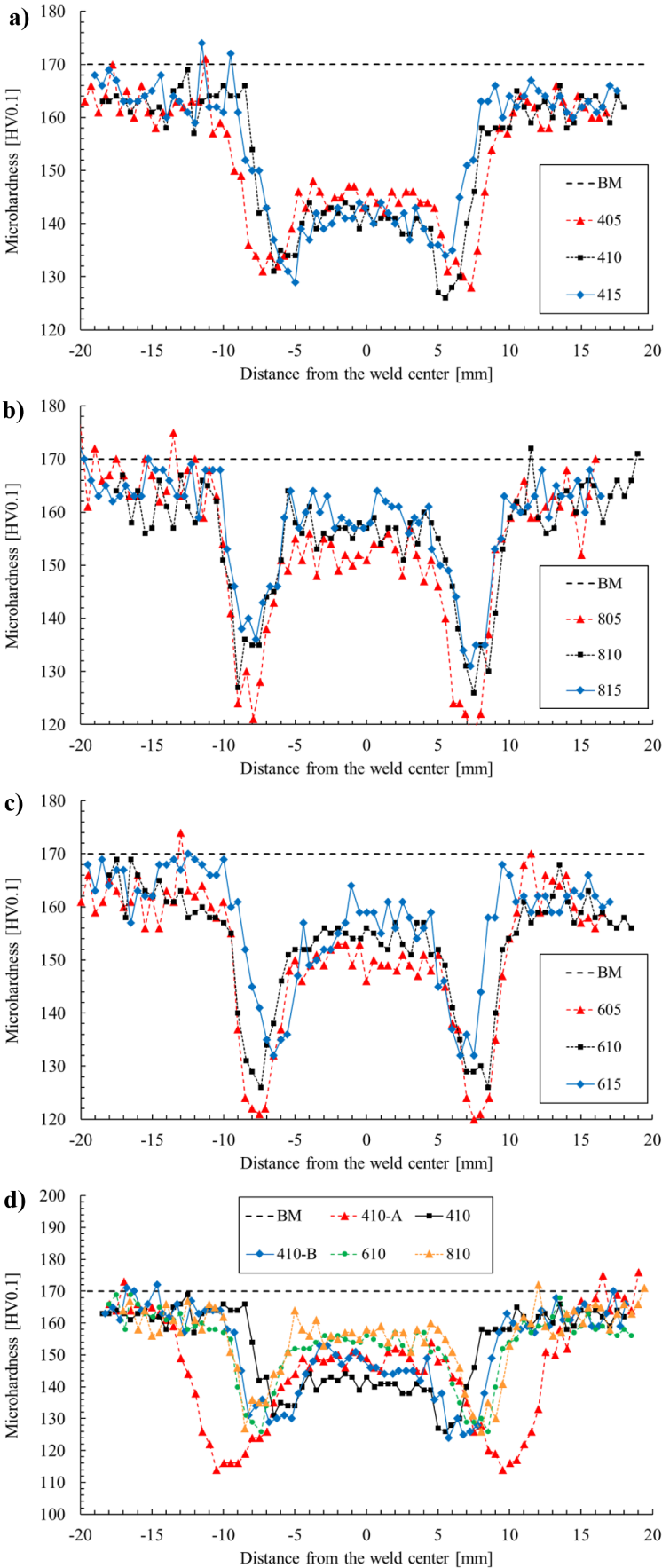


Figure 4. Microhardness distribution for 400 rpm selected samples (a), 600 rpm (b), 800 rpm tool rotation speed (c) and 100 mm/min tool traverse speed (d)

applied water cooling the tensile tests have been performed. The results have been set in graphs in Fig. 5a-d. For samples obtained using the lowest welding speed (50 mm/min), a strong correlation can be observed between the mechanical properties and the tool rotational speed (Fig. 5a). An increase in the tool rotational speed directly leads to a reduction in YS and UTS, while simultaneously improving the ductility of the joint. In this comparison, the highest joint efficiency, corresponding to sample 405 is 84.4% (492.5 MPa), which significantly exceeds the values of air-cooled FSW joints from the previous study [25]. However, for joints produced at higher welding speeds, this trend is reversed, and an increase in tool rotational speed has a beneficial effect on the joint's load-bearing capacity (Fig. 5b,c). Considering the joints from series 410, the impact of the cooling medium on joint efficiency is as follows: 76.7% (448 MPa) for air cooling, 84.1% (491 MPa) for water cooling, and 84.7% (494 MPa) for machining coolant (Fig. 5b). At the same time, among all samples welded at 100 mm/min, samples 410-A and 410-B exhibit significantly higher ductility and lower YS values. This is a direct consequence of the wide and soft heat-affected zones observed in the microhardness distributions of these samples (Fig. 4d). Samples cooled with water, produced at welding speeds of 100 and 150 mm/min, show the same trend of increasing UTS and YS values with higher tool rotational speeds (Fig. 5b,c). It is noteworthy that the highest joint efficiency was observed for sample 815, which is 89% (518 MPa). A similar study on the UWFSW of precipitation-hardened aluminium alloy performed by Sabari et al., showed additional water cooling allows the joint efficiency to be increased by over 15%, with only a slight reduction in ductility [30], which in general overlap with the current study. The comparison of representative tensile curves for joints produced at 100 mm/min is shown in Fig. 5d. Essentially, the tensile curves of FSW joints exhibit a similar pattern, with a noticeable tendency for strain hardening, which is not observed in the base material. Regardless of the welding parameters used, water-cooled samples significantly outperform conventional FSW joints in terms of YS and UTS. The joint cooled with machining coolant is particularly noteworthy, as it not only demonstrates higher strength parameters but also retains high ductility. Saeyang et al. used a cutting fluid for performing UWFSW joints of AA7075-T6 alloy [31], and similarly reported an

increase in ductility compared to conventional FSW. In the literature, there are also reports that cooling the FSW process of AA7075 alloy using liquid nitrogen results in higher ductility [32]. The examined FSW joints tend to fail in the LHZ.

### Fatigue performance

To compare fatigue properties, samples 410-A and 410-B were evaluated. Sample 410-B was selected due to its high joint efficiency of 84.7% (494 MPa) and ductility (6.2%). An additional factor was that, despite its lower YS, it surpassed the 410 joint in strength, suggesting a higher tendency for strain hardening and making it worth investigating in terms of LCF properties. The results presented for the base material and conventional FSW joint (sample 410-A) have been published as a part of the previous work [33]. The changes in stress amplitude and plastic strain amplitude over the number of cycles for the base material, as well as for samples 410-A and 410-B, are illustrated in Fig. 6a,b. At a low total strain amplitude ( $\epsilon_{ac} = 0.35\%$ ), there is a weak tendency for both FSW and UWFSW joints to undergo cyclic hardening (Fig. 6a). This characteristic becomes more pronounced at higher amplitudes ( $\epsilon_{ac} = 0.6\%$ ). The UWFSW joint hardens more significantly, reaching a stress amplitude of approximately 375 MPa, followed by rapid cyclic softening until failure. Although the FSW joint reaches a stress amplitude of around 350 MPa, it exhibits a higher number of cycles to failure. The behaviour of both joint variants contrasts with the base material, which shows only a very weak tendency for cyclic hardening at high total strain amplitudes. The greater susceptibility to plastic deformation of the conventional FSW joint is also evident in the progression of plastic strain amplitude changes in the number of cycles (Fig. 6b). In Fig. 7a and 7b, the stabilized hysteresis loops for the tested samples are shown, along with a comparison of the monotonic and cyclic curves. Analysis of the obtained hysteresis loops reveals that FSW and UWFSW joints exhibit greater susceptibility to deformation energy dissipation compared to the base material (Fig. 7a). In the case of the joint produced using water cooling, the area of the hysteresis loop is significantly smaller than that of the air-cooled counterpart, indicating a markedly lower susceptibility to plastic deformation. The relative positioning of the monotonic and cyclic curves allows for

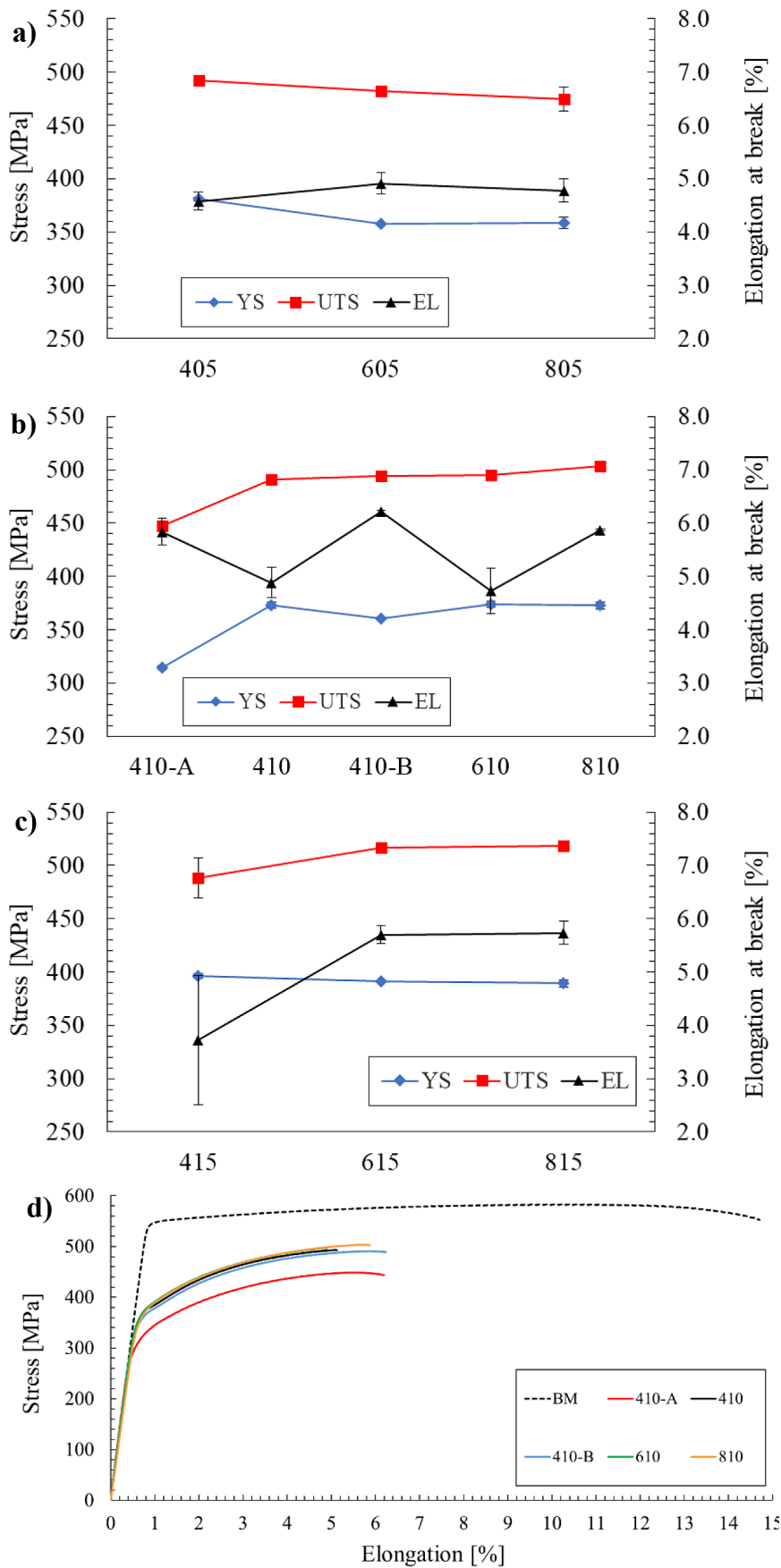


**Figure 5.** Influence of the tool rotation speed on yield strength (YS), ultimate tensile strength (UTS), and elongation at break (EL) for samples produced with 50 mm/min (a), 100 mm/min (b), and 150 mm/min (c) tool traverse speed, together with the comparison of 100 mm/min tensile curves (d)

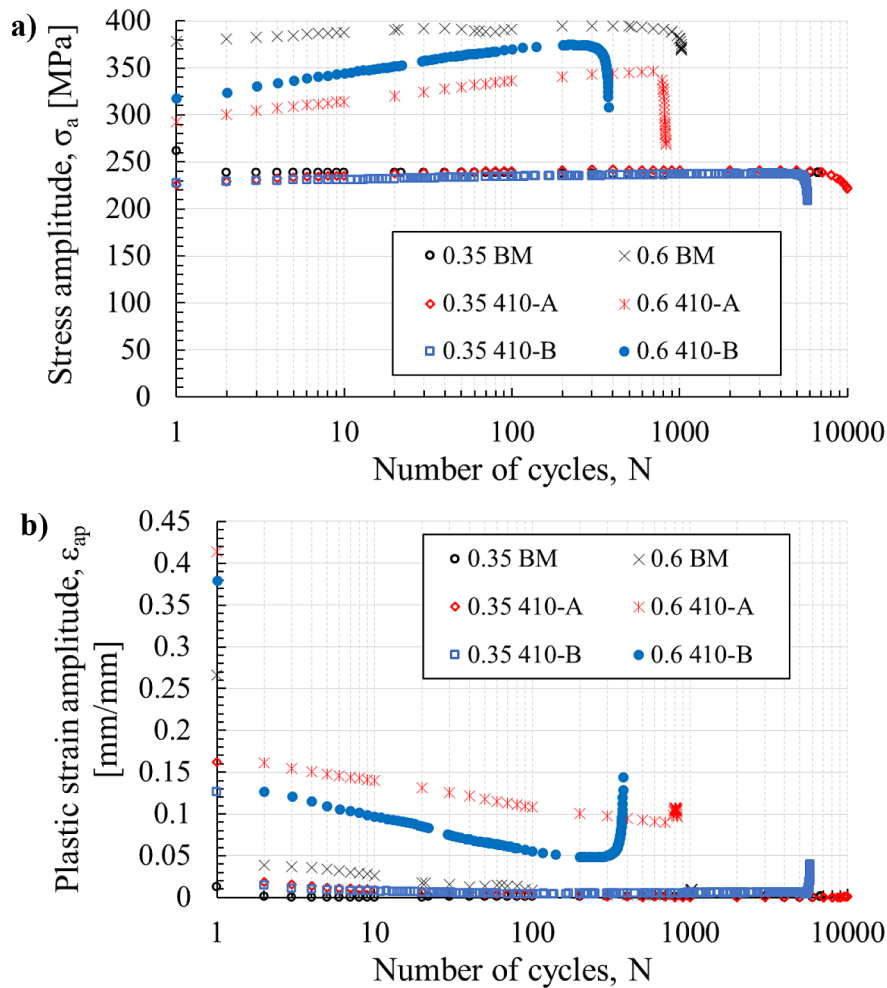


**Figure 6.** Stress amplitude (a) and plastic strain amplitude (b) vs the number of cycles at total strain amplitude of  $\epsilon_{ac} = 0.35\%$  and  $\epsilon_{ac} = 0.6\%$

conclusions about the material’s tendency towards cyclic hardening (Fig. 7b). This also confirms the earlier observations of a greater potential for cyclic strain hardening in the joint produced with water cooling. The monotonic curve is described by the Ramberg-Osgood equation:

$$\epsilon_{ac} = \frac{\sigma_a}{E} + \left(\frac{\sigma_a}{K'}\right)^{\frac{1}{n'}} \quad (1)$$

where:  $\sigma_a$  – stress amplitude,  $E$  – Young modulus,  $K'$  – cyclic strength coefficient and  $n'$  – cyclic strain hardening exponent.

The established parameters are set in Tab. 4. Analysis of the obtained values reveals that both FSW and UWFSW processes significantly affect the parameters of the base material equation. In the case of conventional joints, there is primarily a reduction in the cyclic strength coefficient by approximately 30%, which is a typical phenomenon for FSW joints [34]. The UWFSW joint

exhibits a value of  $K'$  close to that of the base material while also demonstrating a higher cyclic hardening exponent, with an increase of over 40% (Tab. 4). This deviates from the literature reports in this area, which indicate a decrease in the hardening exponent for AA2219-T62 alloy FSW and UWFSW joints [21]. It is worth noting that this cannot be compared with other studies on UWFSW of the 7075-T651 alloy. Additionally, the joint analysed here was made with machining coolant, which has mechanical properties that slightly differ from those of water-cooled joints, e.g. higher ductility (Fig. 5d). Similar to the static tensile test, the fracture of samples subjected to low-cycle fatigue occurred through the LHZ.

All tested samples have been set in the graph below (Fig. 8), which illustrates the relationship between total strain amplitude and the number of reversals to failure. The presented curves (Fig. 8)

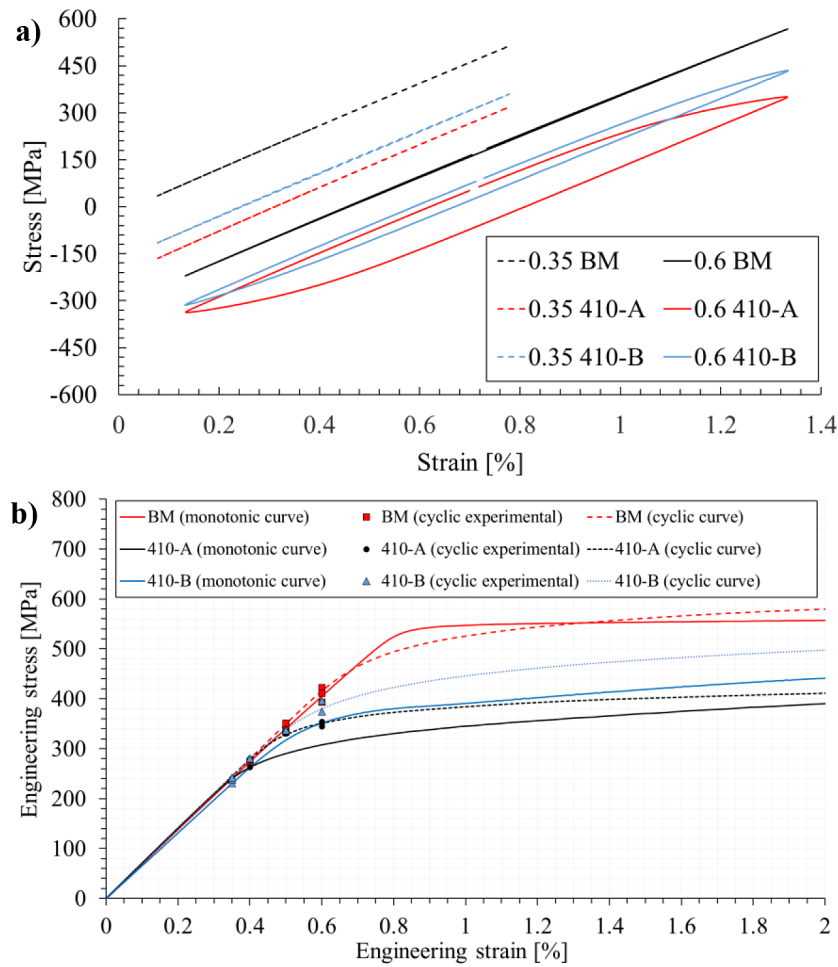


Figure 7. Stabilized hysteresis loops (a) and the comparison of the monotonic and cyclic curves (b)

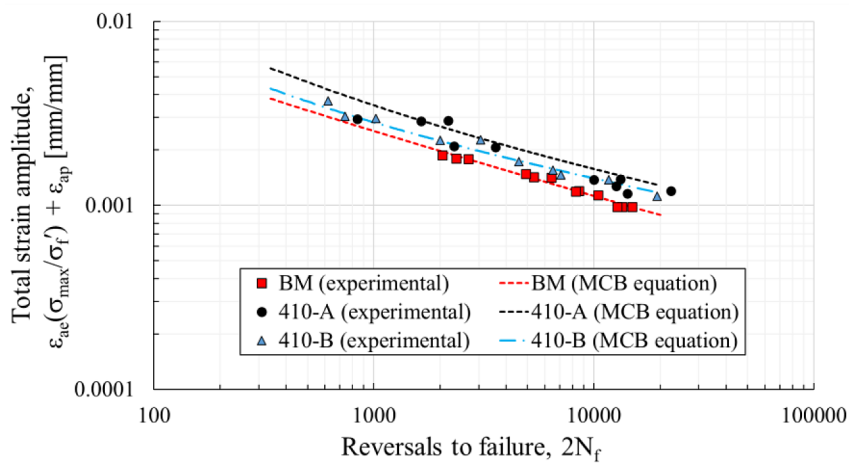


Figure 8. Fatigue strain-life curves

are described by a modification of the Manson-Coffin-Basquin equation, which has performed by Ince and Glinka [35]:

$$\epsilon_{eq,ac} = \frac{\sigma_f'}{E} (2N_f)^{2b} + \epsilon_f' (2N_f)^c \quad (2)$$

where:  $\sigma_f'$  – fatigue strength coefficient,  $b$  – fatigue strength exponent,  $\epsilon_f'$  – fatigue ductility coefficient,  $c$  – fatigue ductility coefficient.

The established parameters are set in Tab. 5. Analysis of the obtained results leads to the

**Table 4.** Established values of Ramberg-Osgood relationship components from Equation (1)

Sample	Cyclic strength coefficient, K'	Cyclic strain hardening exponent, n'
BM	747 MPa	0.0597
410-A	530 MPa	0.0595
410-B	724 MPa	0.0863

**Table 5.** Established values of Manson-Coffin-Basquin relationship components from equation 2

Parameter	BM	410-A	410-B
Fatigue strength coefficient, $\sigma'_f$	1829.5 MPa	923.4 MPa	940.6 MPa
Young modulus, E	70 GPa		
Fatigue strength exponent, b	-0.171	-0.122	-0.125
Fatigue ductility coefficient, $\epsilon_f$	0.1425	0.1971	0.2984
Fatigue ductility exponent, c	-1.019	-0.757	-0.95

conclusion that the curve corresponding to the UWFSW joint is positioned closer to the base material curve than the curve for the air-cooled joint, which should be considered a positive effect (Fig. 8). As a result of the FSW process, components related to fatigue strength are primarily reduced, although this reduction is slightly less significant for UWFSW joints (Table 5). In the case of components related to fatigue ductility, there is a discrepancy with the limited literature reports [21], highlighting the need for further research in this area.

## CONCLUSIONS

The results of the study on the basic mechanical properties of UWFSW butt joints of AA7075-T651 alloy indicate that this is a highly promising direction for further research and potential applications. The main conclusions drawn from the conducted research are:

1. It is possible to produce defect-free, high-quality butt joints using the UWFSW process on 5 mm AA7075-T651 alloy components within a process parameter range of 400 to 800 rpm tool rotational speed and 50 to 150 mm/min tool traverse speed.
2. The use of additional water cooling significantly reduces the width of the HAZ and increases the hardness of the LHZ by an average of approximately 20 HV0.1
3. Regardless of the welding parameters used, UWFSW joints outperform conventional FSW joints of the AA7075-T651 alloy in terms of YS and UTS, with only slightly lower ductility. The use of machining coolant enables the

production of UWFSW joints with higher load-carrying capacity and greater ductility compared to FSW.

4. Under low-cycle fatigue conditions, UWFSW joints exhibit a greater tendency for cyclic hardening, lower plastic strain amplitude, and fewer cycles to failure. The obtained MCB curves indicate that the behaviour of UWFSW joints is more similar to the base material than in the case of conventional FSW joints.

## Acknowledgements

The authors would like to thank Mr. Piotr Anders for performing the photo of the ESAB FSW Legio 4UT machine. This work was financed by Military University of Technology under research project UGB 708/2024.

## REFERENCES

1. Ahmed M.M.Z., El-Sayed Seleman M.M., Fydrych D., Çam G. Friction Stir Welding of Aluminum in the Aerospace Industry: The Current Progress and State-of-the-Art Review. *Materials* 2023, 16, 2971. <https://doi.org/10.3390/ma16082971>
2. Wang G., Zhao Y., Hao Y. Friction stir welding of high-strength aerospace aluminum alloy and application in rocket tank manufacturing. *Journal of Materials Science & Technology* 2018, 34, 1, 73-91. <https://doi.org/10.1016/j.jmst.2017.11.041>
3. Mishra R.S., Mahoney M.W. Friction Stir Welding and Processing. ASM International, Materials Park, OH, USA (2007)
4. Balawender T., Myśliwiec P. Experimental Analysis of FSW Process Forces. *Advances in Manufacturing*

- Science and Technology 2020, 44, 2, 51-56. <https://doi.org/10.2478/amst-2019-0006>
5. Ahmed M. M. Z., El-Sayed Seleman M. M., Fydrych D., Çam G. Review on friction stir welding of dissimilar magnesium and aluminum alloys: Scientometric analysis and strategies for achieving high-quality joints. *Journal of Magnesium and Alloys* 2023, 11, 11, 4082-4127. <https://doi.org/10.1016/j.jma.2023.09.039>.
  6. Gopi S., Mohan D. G., Natarajan E. Mechanical and Corrosion Properties of Friction Stir Welded and Tungsten Inert Gas Welded Phosphor Bronze. *Advances in Materials Science* 2023, 23, 83-98. <https://doi.org/10.2478/adms-2023-0024>.
  7. Iwaszko J., Kudła K. Evolution of Microstructure and Properties of Air-Cooled Friction-Stir-Processed 7075 Aluminum Alloy. *Materials* 2022, 15, 7, 2633. <https://doi.org/10.3390/ma15072633>
  8. Kosturek R., Torzewski J., Joska Z., Wachowski M., Śnieżek L. The influence of tool rotation speed on the low-cycle fatigue behavior of AA2519-T62 friction stir welded butt joints. *Engineering Failure Analysis* 2022, 142, 106756. <https://doi.org/10.1016/j.engfailanal.2022.106756>
  9. Çam G., Mistikoglu S. Recent developments in friction stir welding of Al-alloys. *J. Mater. Eng. Perform.* 2014, 23, 1936–1953. <https://doi.org/10.1007/s11665-014-0968-x>
  10. Li D., Yang X., Cui L., He Fa., Zhang X. Investigation of stationary shoulder friction stir welding of aluminum alloy 7075-T651. *Journal of Materials Processing Technology*, 2015, 222. <https://doi.org/10.1016/j.jmatprotec.2015.03.036>
  11. Patel V., De Backer J., Hindsefelt H., Igestrand M., Azimi S., Andersson J., Säll J. High speed friction stir welding of AA6063-T6 alloy in lightweight battery trays for EV industry: Influence of tool rotation speeds. *Materials Letters* 2022, 318, 132135. <https://doi.org/10.1016/j.matlet.2022.132135>
  12. Joshi A., Gope A., Gope P. C. Effect of post-weld heat treatment on mechanical properties and fatigue crack growth behaviour of friction stir welded 7075-T651 Al alloy. *Theoretical and Applied Fracture Mechanics* 2023, 123, 103714. <https://doi.org/10.1016/j.tafmec.2022.103714>
  13. Wahid M.A., Khan Z.A., Siddiquee A.N. Review on underwater friction stir welding: A variant of friction stir welding with great potential of improving joint properties. *Trans. Nonferrous Met. Soc. China* 2018, 28, 2, 193-219. [https://doi.org/10.1016/S1003-6326\(18\)64653-9](https://doi.org/10.1016/S1003-6326(18)64653-9)
  14. Saravanakumar R., Rajasekaran T., Pandey C. Underwater Friction Stir Welded Armour Grade AA5083 Aluminum Alloys: Experimental Ballistic Performance and Corrosion Investigation. *J. of Mater Eng and Perform* 2023, 32, 10175–10190. <https://doi.org/10.1007/s11665-023-07836-2>
  15. Memon S., Tomków J., Derazkola H.A. Thermo-Mechanical Simulation of Underwater Friction Stir Welding of Low Carbon Steel. *Materials* 2021, 14, 4953. <https://doi.org/10.3390/ma14174953>
  16. Sree Sabari S., Malarvizhi S., Balasubramanian V. Characteristics of FSW and UWFSW joints of AA2519-T87 aluminium alloy: Effect of tool rotation speed. *Journal of Manufacturing Processes* 2016, 22, 278-289. <https://doi.org/10.1016/j.jmapro.2016.03.014>
  17. Liu H.J., Zhang H.J., Yu L. Effect of welding speed on microstructures and mechanical properties of underwater friction stir welded 2219 aluminum alloy. *Materials & Design* 2011, 32, 3, 1548-1553. <https://doi.org/10.1016/j.matdes.2010.09.032>
  18. Zhang H.J., Liu H.J., Yu L. Microstructure and mechanical properties as a function of rotation speed in underwater friction stir welded aluminum alloy joints. *Materials & Design* 2011, 32, 8-9, 4402-4407. <https://doi.org/10.1016/j.matdes.2011.03.073>
  19. Rouzbehani R., Kokabi A.H., Sabet H., Paidar M., Ojo O.O. Metallurgical and mechanical properties of underwater friction stir welds of Al7075 aluminum alloy. *Journal of Materials Processing Technology* 2018, 262, 239-256. <https://doi.org/10.1016/j.jmatprotec.2018.06.033>
  20. Byakov A. V., Eremin A. V., Shah R. T., Burkov M. V., Lyubutin P. S., Panin S. V., Maruschak P. O., Menou A., Bencheikh L. Estimating mechanical state of AA2024 specimen under tension with the use of Lamb wave based ultrasonic technique. *Molecular Crystals and Liquid Crystals* 2017, 655, 1, 94–102. <https://doi.org/10.1080/15421406.2017.1360700>
  21. Xu W.F., Liu J.H., Chen D.L., Luan G.H. Low-cycle fatigue of a friction stir welded 2219-T62 aluminum alloy at different welding parameters and cooling conditions. *Int J Adv Manuf Technol* 2014, 74, 209-218. <https://doi.org/10.1007/s00170-014-5988-z>
  22. Khalaf H.I., Al-Sabur R., Abdullah M.E., Kubit A., Derazkola H.A. Effects of Underwater Friction Stir Welding Heat Generation on Residual Stress of AA6068-T6 Aluminum Alloy. *Materials* 2022, 15, 2223. <https://doi.org/10.3390/ma15062223>
  23. Venugopal A., Mohammad R., Koslan M.F.S., Shafie A., Ali A., Eugene O. Structure Life Extension towards the Structural Integrity of Sukhoi Su-30MKM. *Materials* 2021, 14, 19, 5562. <https://doi.org/10.3390/ma14195562>
  24. Mahoney M.W., Rhodes C.G., Flintoff J.G. et al. Properties of friction-stir-welded 7075 T651 aluminum. *Metall Mater Trans A* 1998, 29, 1955–1964. <https://doi.org/10.1007/s11661-998-0021-5>
  25. Kosturek R., Torzewski J., Wachowski M., Śnieżek L. Effect of Welding Parameters on Mechanical Properties and Microstructure of Friction Stir

- Welded AA7075-T651 Aluminum Alloy Butt Joints. *Materials* 2022, 15, 17, 5950. <https://doi.org/10.3390/ma15175950>
26. ASTM E8/E8M-13a, Standard test methods for tension testing of metallic materials, ASTM Int. 2013, 1-28. [https://doi.org/10.1520/E0008\\_E0008M-11](https://doi.org/10.1520/E0008_E0008M-11)
27. ISO 12106:2017, Metallic materials — Fatigue testing — Axial-strain-controlled method, ISO 2017, 1-42.
28. Kosturek R., Śnieżek L., Torzewski J., Wachowski M. The influence of welding parameters on macrostructure and mechanical properties of Sc-modified AA2519-T62 FSW joints. *Manufacturing Review* 2020, 7, 28. <https://doi.org/10.1051/mfreview/2020025>
29. Zhang J., Upadhyay P., Hovanski Y., Field D. High-Speed Friction Stir Welding of AA7075-T6 Sheet: Microstructure, Mechanical Properties, Micro-texture, and Thermal History. *Metallurgical and Materials Transactions A* 2017, 49. <https://doi.org/10.1007/s11661-017-4411-4>
30. Sabari S., Malarvizhi S., Balasubramanian V. Influences of tool traverse speed on tensile properties of air cooled and water cooled friction stir welded AA2519-T87 aluminium alloy joints. *Journal of Materials Processing Technology* 2016, 237. <https://doi.org/10.1016/j.jmatprotec.2016.06.015>
31. Saeyang P., Chanpariyavatevong A., Lamkham K., Siwadamrongpong S., Tantrairatn S. Influence of Cooling Methods in Friction Stir Welding of 7075 Aluminum Alloy. *International Journal of Engineering Research in Mechanical and Civil Engineering* 2023, 10, 4. <https://doi.org/01.1617/vol10/iss4/pid18053>
32. Iwaszko J. New Trends in Friction Stir Processing: Rapid Cooling—A Review. *Transactions of the Indian Institute of Metals*, 2022, 75, 1681–1693. <https://doi.org/10.1007/s12666-022-02552-2>
33. Kosturek R., Śnieżek L., Torzewski J., Ślęzak T., Lewczuk R. Influence of post-weld explosive treatment on low cycle fatigue of AA7075-T651 friction stir welded joint. *Theoretical and Applied Fracture Mechanics* 2024, Volume 133, Part A, October 2024, 104574. <https://doi.org/10.1016/j.tafmec.2024.104574>
34. Feng A.H., Chen D.L., Ma Z.Y. Microstructure and Low-Cycle Fatigue of a Friction-Stir-Welded 6061 Aluminum Alloy. *Metall Mater Trans A* 2010, 41, 2626–2641. <https://doi.org/10.1007/s11661-010-0279-2>
36. Ince A., Glinka G. A modification of Morrow and Smith–Watson–Topper mean stress correction models. *Fatigue & Fracture of Engineering Materials & Structures* 2021, 34, 854–867. <https://doi.org/10.1111/j.1460-2695.2011.01577.x>